Multicritical phase diagrams of the Blume-Emery-Griffiths model with repulsive biquadratic coupling including metastable phases

Cesur Ekiz and Mustafa Keskin
Department of Physics, Erciyes University, 38039 Kayseri, Turkey

(Received 10 October 2001; revised manuscript received 1 February 2002; published 12 August 2002)

We investigate the thermal variations of the spin-1 Blume-Emergy-Griffiths model with the repulsive biquadratic interaction by using the lowest approximation of the cluster-variation method. Besides the stable branches of the order parameters, we obtain the metastable and unstable parts of these curves and also find phase transitions of the metastable branches of the order parameters. The classification of the stable, metastable, and unstable states is made by comparing the free-energy values of these states. We also study the dynamics of the model by the path probability method in order to make sure that we find and define the metastable and unstable branches of the order parameters completely and correctly. This is done by studying the relaxation of the order parameters and as well as expressing the solution of the dynamic equations by means of the flow diagrams. Finally, we present the metastable phase diagrams in addition to the equilibrium phase diagrams in $(kT/J,D/J)$ and $(kT/J,K/J)$ planes.

DOI: 10.1103/PhysRevB.66.054105 PACS number(s): 64.60.Cn, 64.60.Kw, 05.70.Fh, 75.10.Hk

I. INTRODUCTION

The Blume-Emery-Griffiths (BEG) model[1] is a spin-1 Ising model with bilinear (J) and biquadratic (K) nearest-neighbor pair interactions in which a single-ion anisotropy parameter (D) is included. The BEG model has attracted a great deal of attention since it was originally proposed to describe phase separation and superfluid ordering in helium mixtures. It has subsequently been used to describe phase transitions in simple and multicomponent fluids, microemulsions, semiconductor alloys, the reentrant phenomenon in phase diagrams, electron conduction models, and martensitic transformation to quote only a few. Moreover, the BEG model has also played an important guiding role in the development of microscopic models for adsorbed systems and in the renormalization-group theory of Potts transitions.

The BEG model is defined by the following Hamiltonian:

$$H=-J\sum_{\langle ij\rangle} S_iS_j-K\sum_{\langle ij\rangle} S_i^2S_j^2+D\sum_i S_i^2, \qquad (1)$$

where $S_i=\pm 1,0$ is at each site i of a lattice, each site has z nearest neighbors, and $\langle ij\rangle$ indicates summation over all pairs of nearest-neighbor sites.

The phase diagrams of the BEG model for $K/J\geqslant 0$ have been studied by the mean-field approximation,[1–3] the position-space renormalization-group method,[4] the cluster-variation method,[5,6] series-expansion methods,[7] the transfer-matrix method,[8] the constant coupling approximation,[9] linear-chain approximation,[10] and on the Bethe lattice using exact recursion equations.[11] Recently we also studied the BEG model for J and $K>0$ and obtained the metastable and unstable states besides the stable state.[12] We found that the metastable and unstable branches of the order parameters undergo first- or second-order phase transitions. We also presented the metastable phase diagram of the BEG model in addition to the equilibrium phase diagram.[13]

On the other hand the BEG model with repulsive biquadratic coupling, i.e., $K/J<0$ is now a subject of intense study.[14] For example, a study of the global phase diagram of the BEG model for $K<0$ was made by using the mean-field approximation (MFA),[15] showing a variety of interesting features, including single and double reentrancy regions and ferrimagnetic phases. In a renormalization-group calculation of the model for $K/J<0$, the phase diagrams[16] are different from the ones of the MFA. The main discrepancy is that no ferrimagnetic phase is seen. Furthermore, for repulsive biquadratic interaction, the BEG model has been investigated by the Monte Carlo method,[17] cluster-variation method,[18] and using a Monte Carlo renormalization group.[19] In this context, the exact solutions of the BEG model on the Bethe lattice, and the honeycomb and square lattice in two dimensions are worth mentioning.[20] The phase diagrams obtained by the above-mentioned works are only the equilibrium phase diagrams.

In spite of these studies, the equilibrium properties of the BEG model for $K/J<0$ is not investigated using the lowest approximation of the cluster-variation method (LACVM) extensively. Especially, the metastable and unstable branches of the order parameters and their phase transitions are not examined in depth. Moreover the metastable phase diagrams of the model in addition to the equilibrium phase diagrams were also not calculated. Therefore, the purpose of this work is to study the behavior of the thermal variation of the order parameters and to obtain the metastable and unstable branches of the order parameters and to investigate their phase transitions for repulsive biquadratic interaction. We also study the dynamics of the model in order to make sure that we find and classify the metastable and unstable branches of the order parameters completely and correctly. Finally, we present the metastable phase diagrams of the BEG model in addition to the equilibrium phase diagrams.

It is worthwhile to mention that the metastable and unstable states have been found in many physical systems experimentally and theoretically. For example, the BEG model Hamiltonian with zero-crystal-field interaction theoretically have been studied for zero magnetic field,[21] an external magnetic field,[22] and as well as for magnetic fields due to the

dipole and quadrupole moments.[23] Moreover, the metastable phase diagrams are presented in addition to the equilibrium phase diagram for some alloys,[24–26] semiconductors,[27,28] polymers,[29] water,[30] and a ternary system.[31] The unstable continuation of the second-order phase-transition line is also mentioned in $(A^{III}B^{V})_{1-X}C_{2X}^{IV}$ semiconductor alloys, theoretically in addition to the metastable and equilibrium phase diagram.[32] On the other hand, the BEG model has been used to calculate the metastable phase diagram of the Cu-Al-Mn shape-memory alloys,[26] semiconductor alloys,[28] as well as the ternary system.[31] Moreover, the unstable continuation of the second-order phase-transition line is presented by using the BEG model in semiconductor alloys.[32]

The outline of this work is as follows. In Sec. II, we define the model briefly and obtain its solutions at equilibrium within the LACVM. The equilibrium properties of the system are investigated in Sec. III. The dynamics of the model is studied by the path probability method in Sec. IV. In Sec. V, transition temperatures are calculated precisely and metastable phase diagrams are presented in addition to the equilibrium phase diagrams. Section VI contains the summary and conclusion.

II. MODEL AND METHOD

The BEG model is defined as a two-sublattice model, with spin variables $S_i=\pm 1,0$ and $S_j=\pm 1,0$ on sites of sublattices A and B, respectively. The average value of each of the spin states will be denoted by X_1^A, X_2^A, and X_3^A on the sites of sublattice A and X_1^B, X_2^B, and X_3^B on the sublattice B, which are also called the state or point variables. X_1^A and X_1^B are the fractions of the spin value $+1$ on A and B sublattices, respectively, and X_2^A and X_2^B are the fractions of the spins that have value 0 on A and B sublattices, respectively, and X_3^A and X_3^B are the fractions of the spins that have the value -1 on A and B sublattices, respectively. These variables obey the following two normalization relations for A and B sublattices,

$$\sum_{i=1}^{3} X_i^A=1$$

and

$$\sum_{j=1}^{3} X_j^B=1. \tag{2}$$

However, in order to account for the possible two-sublattice structure, we need four long-range order parameters, which are introduced as follows: $M_A=\langle S_i\rangle_A$, $Q_A=\langle S_i^2\rangle_A$, $M_B=\langle S_j\rangle_B$, and $Q_B=\langle S_j^2\rangle_B$ for A and B sublattices, respectively. M_A and M_B are the average magnetizations which is the excess of one orientation over the other orientation, called magnetizations, and Q_A and Q_B are the quadrupolar moments which is the average squared magnetizations for A and B sublattices, respectively. The values of these stable branches of the order parameters define four phases with different symetry. These are (i) the paramagnetic phase (p) with $M_A=M_B=0, Q_A=Q_B$, (ii) the ferromagnetic phase (f) with $M_A=M_B\neq 0, Q_A=Q_B$, (iii) the antiquadrupolar or staggered quadrupolar phase (a) with $M_A=M_B=0$, $Q_A\neq Q_B$, and (iv) the ferrimagnetic phase (i) with $M_A\neq M_B\neq 0, Q_A\neq Q_B$.

The order parameters can be expressed in terms of the internal variables and are given by

$$\begin{aligned} M_A&=\langle S_i^A\rangle=X_1^A-X_3^A,\\ Q_A&=\langle (S_i^A)^2\rangle=X_1^A+X_3^A,\\ M_B&=\langle S_j^B\rangle=X_1^B-X_3^B,\\ Q_B&=\langle (S_j^B)^2\rangle=X_1^B+X_3^B. \end{aligned} \tag{3}$$

Using Eqs. (2) and (3), the internal variables can be expressed as linear combinations of the order parameters,

$$\begin{aligned} X_1^A&=\frac{1}{2}(Q_A+M_A), \quad X_2^A=(1-Q_A),\\ X_3^A&=\frac{1}{2}(Q_A-M_A),\\ X_1^B&=\frac{1}{2}(Q_B+M_B), \quad X_2^B=(1-Q_B),\\ X_3^B&=\frac{1}{2}(Q_B-M_B). \end{aligned} \tag{4}$$

The Hamiltonian of such a two-sublattice BEG model is

$$H=-J\sum_{\langle ij\rangle} S_iS_j-K\sum_{\langle ij\rangle} S_i^2S_j^2+D\left(\sum_i S_i^2+\sum_j S_j^2\right). \tag{5}$$

The equilibrium properties of the system are determined by the lowest approximation of the cluster-variation method[33] (LACVM) which is identical to the mean-field approximation. The method consists of the following three steps: (i) consider a collection of weakly interacting systems and define the internal variables; (ii) obtain the weight factor in terms of the internal variables; and (iii) find the free-energy expression and minimize it. The LACVM, in spite of its limitations, is an adequate starting point. Within this theoretical framework it is easy to determine the complete phase diagrams and find some outstanding features in the temperature dependencies of order parameters and as well as obtain the metastable portion of the phase diagrams.

The weight factors W^A and W^B can be expressed in terms of the internal variables for the A and B sublattices, respectively, as

$$W^A=\frac{N^A!}{\prod_{i=1}^{3}(X_i^AN^A)!}$$

and

$$W^B=\frac{N^B!}{\prod_{j=1}^{3}(X_j^B N^B)!}, \tag{6}$$

where N^A and N^B are the number of lattice points on the A and B sublattices, respectively. On the other hand, a simple expression for the internal energy of the system is found by working out Eq. (5) in the lowest approximation of the cluster-variation method.

This leads to

$$\frac{E}{N}=-JM_AM_B-KQ_AQ_B+D(Q_A+Q_B). \tag{7}$$

Substituting Eq. (3) into Eq. (7), the internal energy per site can be written as

$$\frac{E}{N}=-J(X_1^A-X_3^A)(X_1^B-X_3^B) -K(X_1^A+X_3^A)(X_1^B+X_3^B)+D\{(X_1^A+X_3^A)+(X_1^B+X_3^B)\}, \tag{8}$$

where $N=N^A+N^B$ is the total lattice points.

Using the definition of the entropy $S_e(S_e=k\ln W)$ with the Stirling approximation, the free energy $F(F=E-TS)$ per site can now be found as

$$\Phi=\frac{F}{N}=-JM_AM_B-KQ_AQ_B+D(Q_A+Q_B) +\frac{1}{\beta}\left(\sum_{i=1}^{3}X_i^A\ln X_i^A+\sum_{j=1}^{3}X_j^B\ln X_j^B\right)+\lambda^A\left(1-\sum_{i=1}^{3}X_i^A\right) +\lambda^B\left(1-\sum_{j=1}^{3}X_j^B\right), \tag{9}$$

where λ^A and λ^B are introduced to maintain the normalization condition, $\beta=1/kT$, T is the absolute temperature, and k is the Boltzmann factor.

Thus, the self-consistent equations for the four long-range order parameters, namely, M_A, Q_A, M_B, and Q_B are therefore obtained by

$$\frac{\partial\Phi}{\partial X_i^A}=0 \quad (i=1,2,3)$$

and

$$\frac{\partial\Phi}{\partial X_j^B}=0 \quad (j=1,2,3). \tag{10}$$

Using Eqs. (3), (9), and (10), the self-consistent equations are found to be

$$M_A=\frac{2\sinh(\beta JM_B)}{\exp\beta(D-KQ_B)+2\cosh(\beta JM_B)},$$

$$Q_A=\frac{2\cosh(\beta JM_B)}{\exp\beta(D-KQ_B)+2\cosh(\beta JM_B)},$$

$$M_B=\frac{2\sinh(\beta JM_A)}{\exp\beta(D-KQ_A)+2\cosh(\beta JM_A)},$$

$$Q_B=\frac{2\cosh(\beta JM_A)}{\exp\beta(D-KQ_A)+2\cosh(\beta JM_A)}, \tag{11}$$

where D/J and K/J are called the ratio of the coupling constant. We are now able to examine the behavior of the order parameters of the two-sublattice BEG model with repulsive biquadratic coupling by solving of the self-consistent equations, i.e., Eq. (11), numerically. In the following section, we shall examine the thermal variations of the system.

III. THERMAL VARIATIONS

In this section, we shall study the temperature dependencies of the order parameters M_A, Q_A, M_B, and Q_B by solving four nonlinear equations, namely, the set of self-consistent equations, i.e., Eq. (11), numerically. These equations are solved by the Newton-Raphson method[34] and thermal variations of the order parameters for several values of D/J and K/J are plotted in Figs. 1–6. In the figures, the subscript 1 denotes the stable states (solid lines), subscript 2 corresponds to metastable states (dash-dotted lines), and 3 to unstable states (dashed lines). This classification is done by matching the free-energy values of these states. T_c or $T_{c'}$ and T_t are the critical or the second-order phase-transition and the first-order phase-transition temperatures for the stable branches of the order parameters, respectively. T_{fi} and T_{if} are the second-order phase-transition temperatures from the ferromagnetic phase to the ferrimagnetic phase and from the ferrimagnetic phase to the ferromagnetic phase, respectively, for the stable branches of order parameters. T_{t2} and T_{c2} or $T_{c2'}$ are the first- and second-order phase-transition temperatures for the metastable branches of the order parameters, respectively. T_{t2} is the first-order phase-transition temperature where the discontinuity occurs first for the metastable branches of the order parameters. Finally, T_u is the upper limit of the stability temperature in which the discontinuity occurs first for the stable branches of the order parameters. Therefore, the transitions at T_{t2} and T_u are based on the same mechanism.

The behavior of the temperature dependence of the order parameters depends on D/J and K/J values and, by matching the free-energy values of the solutions of the order parameters, the following six main topological different types of behaviors are found:

A. Type 1

For $D/J=0.49$ and $K/J=0.0$, the stable values of the magnetizations, namely, M_{A1},M_{B1}, decrease to zero discontinuously, hence a first-order phase-transition occurs, seen in Fig. 1(a). The first-order phase transition temperature T_t for the stable branch of magnetization is indicated by an arrow and T_u is the upper limit of the stability temperature in Fig.

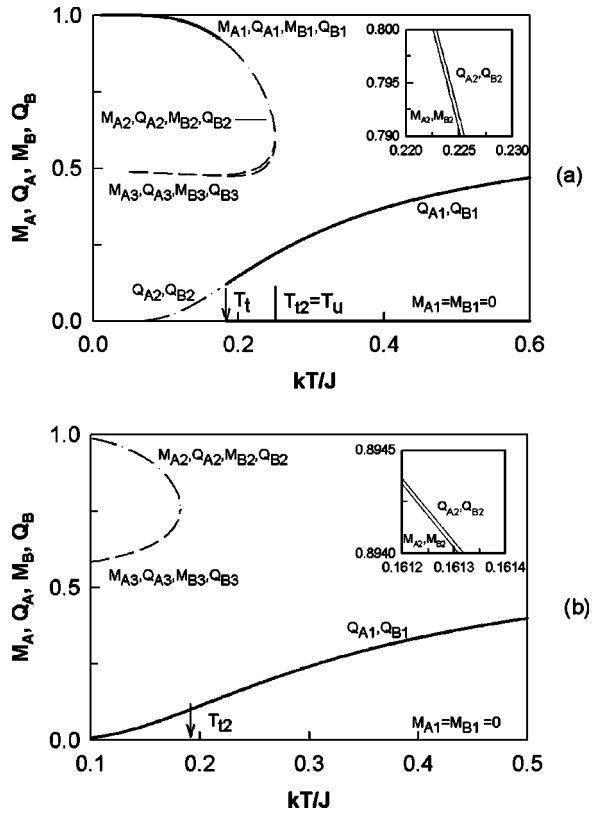

FIG. 1. The temperature dependencies of the order parameters. Subscript 1 indicates the stable state (solid lines), 2 the metastable state (dash-dotted lines), and 3 the unstable state (dashed lines). T_t and T_{t2} are the first-order phase-transition temperatures for the stable and metastable branches of the order parameters, respectively. (a) A first-order phase transition for the stable branch of the order parameters for $D/J=0.49$ and $K/J=0.0$. (b) A first-order phase transition for the metastable branch of the order parameters for $D/J=0.55$ and $K/J=0.0$.

1(a). The stable branches of the order parameters become metastable after T_t, seen in the figure.

For $D/J=0.55$ and $K/J=0.0$, the metastable branches of the order parameters, i.e., M_{A2}, M_{B2}, Q_{A2}, and Q_{B2}, decrease to zero discontinuously, therefore a first-order phase transition occurs at $T_{t2}=0.183$ for M_{A2}, M_{B2}, Q_{A2}, and Q_{B2}, and below T_{t2} the unstable branches of order parameters also exist, seen in Fig. 1(b). It should be mentioned that the stable branches of the quadrupole order parameters do not undergo any phase transitions and the stable branches of the magnetizations are equal to zero. It is worthwhile to mention that in order to distinguish M and Q we included inset figures in Figs. 1(a) and 1(b).

B. Type 2

For $D/J=0.413$ and $K/J=-0.15$, the temperature dependence of the order parameters is similar to Fig. 1(a) but only differ from Fig. 1(a) in that the stable branches of the order parameters undergo two successive second-order phase transitions, i.e., at $T_c=0.252$ and $T_{c'}=0.337$ in addition to the first-order phase transition at $T_t=0.188$, seen in Fig. 2.

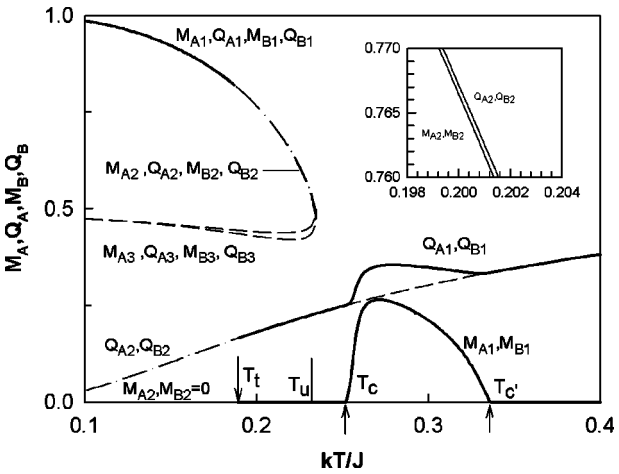

FIG. 2. The temperature dependence of the order parameters exhibiting a first-order phase transition and the two successive second-order phase transitions for the stable branches of the order parameters for $D/J=0.413$ and $K/J=-0.15$. T_t and T_u represent the first-order phase transition for the stable states and the upper limit stability temperature, respectively. T_c and $T_{c'}$ represent the second-order phase-transition temperatures for the stable branches of order parameters.

C. Type 3

For $D/J=-0.3$ and $K/J=-1.5$, the stable values of quadrupolar order parameters undergo a first-order antiquadrupolar phase transition at T_t, seen in Fig. 3. On the other hand, the stable branches of the magnetizations undergo a second-order ferromagnetic phase transition at T_c. Therefore, the system experiences the following phase changes: From the antiquadrupolar (a) phase to the ferromagnetic (f) phase and then from the ferromagnetic (f) phase to the paramagnetic (p) phase, as shown in Fig. 3. Moreover, the metastable branches of quadrupolar order parameters, Q_{A2} and Q_{B2}, undergo a second-order antiquadrupolar phase transition at $T_{c2}=0.374$.

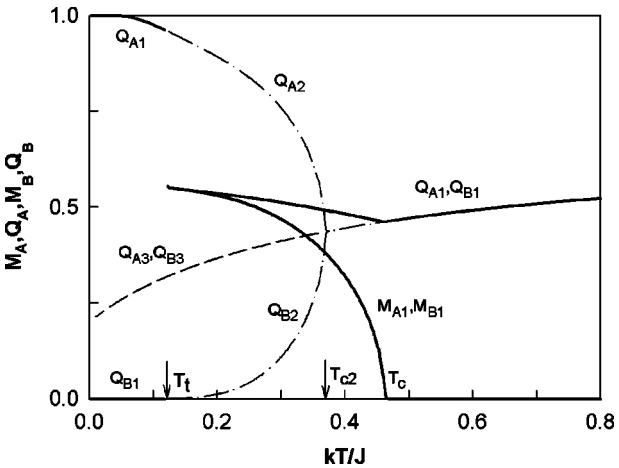

FIG. 3. The temperature dependence of the order parameters exhibiting the first-order antiquadrupolar phase transition and the second-order ferromagnetic phase transitions for $D/J=-0.3$ and $K/J=-1.5$. The metastable quadrupolar order parameters also undergo a second-order antiquadrupolar phase transition at T_{c2}.

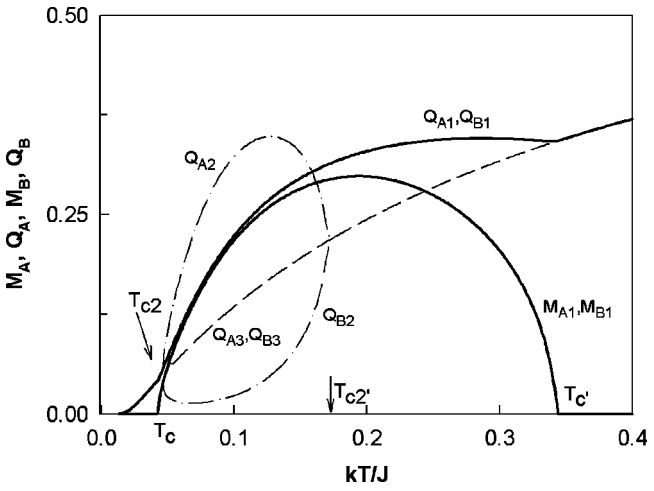

FIG. 4. The temperature dependencies of the order parameters for $D/J=0.12$ and $K/J=-1.0$. T_c and $T_{c'}$ are the second-order ferromagnetic phase transition for the stable branches of order parameters, and T_{c2} and $T_{c2'}$ are the second-order antiquadrupolar phase-transition temperatures for the metastable quadrupolar order parameters.

D. Type 4

For $D/J=0.12$ and $K/J=-1.0$, the stable branches of order parameters undergo two successive second-order ferromagnetic phase transitions, the phase transition from the quadrupolar (q) phase to ferromagnetic (f) phase at $T_c=0.042$ and then from the (f) phase to (p) phase at $T_{c'}=0.345$ as temperature increases, seen in Fig. 4. Moreover, the metastable branches of the quadrupolar order parameters, Q_{A2} and Q_{B2}, undergo two successive second-order antiquadrupolar phase transitions at $T_{c2}=0.044$ and $T_{c2'}=0.177$, respectively.

E. Type 5

In this type, the following three different subtypes have been obtained:

(i) Figure 5(a) represents the temperature dependence of the order parameters for $K/J=-3.0$ and $D/J=-3.0$. The stable branches of the magnetizations decrease to zero continuously as the temperature increases, hence the second-order ferromagnetic phase transition occurs at $T_c=0.8095$, seen in Fig. 5(a). However, the metastable branches of quadrupolar order parameters, Q_{A2} and Q_{B2}, undergo a single second-order antiquadrupolar phase transition at $T_{c2}=0.352$.

(ii) For $K/J=-3.0$ and $D/J=-2.15$, the stable branches of the order parameters experience three successive second-order phase transitions: First, the phase transition from the ferromagnetic (f) phase to ferrimagnetic (i) phase at $T_{fi}=0.0625$, second, from the (i) phase to (f) phase at $T_{if}=0.265$, and finally, from the (f) phase to (p) phase at $T_c=0.697$ as temperature increases, as seen in Fig. 5(b). Moreover, the metastable branches of quadrupolar order parameters, Q_{A2} and Q_{B2}, undergo a single second-order antiquadrupolar phase transition at $T_{c2}=0.646$.

(iii) For $K/J=-3.0$ and $D/J=0.2$, the stable branches of quadrupolar order parameters, Q_{A1} and Q_{B1}, undergo two successive second-order antiquadrupolar phase transitions, the phase transition from the quadrupolar (q) phase to antiquadrupolar (a) phase at $T_c=0.055$ and then from the (a) phase to (p) phase at $T_{c'}=0.595$ as temperature increases, illustrated in Fig. 5(c). Moreover, there are not any branches of magnetizations in this case.

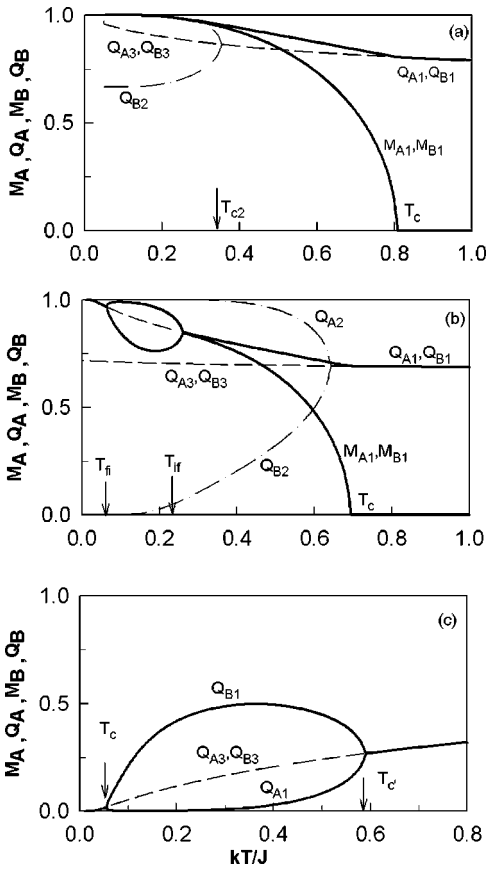

FIG. 5. Temperature dependence of the order parameters for constant $K/J=-3.0$ and various values of the parameter D/J. (a) The second-order ferromagnetic phase transition for the stable branches of the magnetization, M_{A1} and M_{B1}, and the second-order antiquadrupolar phase transition for the metastable branches of the quadrupolar order parameters, Q_{A2} and Q_{B2}, for $D/J=-3.0$. T_c and T_{c2} are the second-order phase-transition temperatures for M_{A1}, M_{B1}, Q_{A2}, and Q_{B2}, respectively. (b) Two successive second-order ferrimagnetic phase transitions and one ferromagnetic phase transition of stable order parameters for $D/J=-2.15$. The metastable quadrupolar order parameters, Q_{A2} and Q_{B2}, also undergo a single second-order antiquadrupolar phase transition at T_{c2}. T_{fi} and T_{if} are the second-order phase-transition temperatures from the ferromagnetic phase to the ferrimagnetic phase and from the ferrimagnetic phase to the ferromagnetic phase, respectively, for the stable branches of order parameters. (c) Two successive second-order antiquadrupolar phase transitions of stable quadrupolar order parameters, Q_{A1} and Q_{B1}, for $D/J=0.2$.

F. Type 6

Figure 6 shows the temperature dependence of the order parameters for $D/J=0.0$ and $K/J=-0.9$. We find a second-order ferromagnetic phase transition for the stable branches

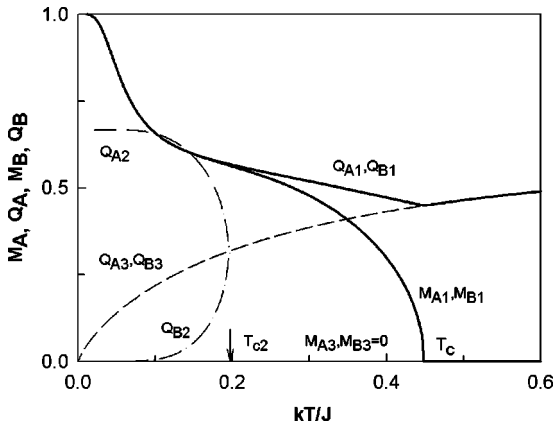

FIG. 6. The temperature dependence of the order parameters exhibiting a second-order ferromagnetic phase transition for the stable branches of the magnetization and second-order antiquadrupolar phase transition for the metastable branches of the quadrupolar order parameters for $D/J=0.0$ and $K/J=-0.9$.

of magnetizations at $T_c=0.4525$. Furthermore, one observes a single second-order antiquadrupolar phase transition for the metastable branches of the quadrupolar order parameters, Q_{A2} and Q_{B2}, at $T_{c2}=0.198$. It should be mentioned that this type is similar to type 5(i), but at zero temperature $Q_{A3}=Q_{B3}=Q_{B2}=0.0$ and $Q_{A2}=2/3$. On the other hand in type 5(i), at zero temperature $Q_{A3}=Q_{B3}=Q_{A2}=1.0$ and $Q_{B2}=2/3$, as seen Fig. 5(a).

IV. DYNAMICS OF THE SYSTEM

In this section, we study dynamics of the BEG model by the path probability method (PPM),[35,36] since the metastable behavior is a dynamical behavior. In this study we have checked all the solutions, which were obtained within the LACVM, and as well as their classifications. The PPM is the natural extension into the time domain of the cluster-variation method and provides a systematic derivation of the rate equations for successive approximations which are well known in the equilibrium statistical mechanics. It has been successfully applied to describe the nonequilibrium behavior of a number of homogeneous and inhomogeneous stationary systems such as substitutional diffusion in ordered systems,[37] diffusion and ionic conductivity in solid electrolytes,[38] the kinetics of the order-disorder transformation in bcc (body-centered-cubic) alloys,[39] a binary alloy,[40] a spin-1/2 Ising model,[41] spin-1 Ising systems,[42,43] phonon and atomic diffusion systems,[44] a ternary system[45] and the microscobic mechanism of the current-induced domain conversion phenomena on the Si (001) vicinal surface.[46] We should also mention that efforts have been made to show how the PPM can be used to evaluate atomistic parameters combined with experiments.[47]

In this method the rate of change of the state variables is written as

$$\frac{dX_i}{dt}=\sum_{i\neq j}(\mathrm{X}_{ji}-\mathrm{X}_{ij}), \tag{12}$$

where X_{ij} is the path probability rate for the system to go from state i to j. The coefficients X_{ij} are the product of three factors: k_{ij} the rate constants with $k_{ij}=k_{ji}$, a temperature-dependent factor which guarantees that the time-independent state is the equilibrium state, and a third factor which is the fraction of the system that is in the state i, e.g., X_i. Detailed balancing requires that

$$\mathrm{X}_{ij}=\mathrm{X}_{ji}. \tag{13}$$

The following two options were introduced by Kikuchi:[35]

$$\text{(A)}\quad \mathrm{X}_{ij}=k_{ij}Z^{-1}\exp\left[-\frac{\beta}{2}\left(\frac{\partial E}{\partial X_i}-\frac{\partial E}{\partial X_j}\right)\right], \tag{14a}$$

$$\text{(B)}\quad \mathrm{X}_{ij}=k_{ij}Z^{-1}\exp\left[-\beta\left(\frac{\partial E}{\partial X_j}\right)\right], \tag{14b}$$

which both fulfill the necessary requirements expressed by Eq. (13), and Z is the partition function and E the internal energy which is given in Sec. II. Assumption A is called recipe I and assumption B is called recipe II by Kikuchi.[35] There are two rate constants in the model and can be easily defined in the language of a lattice gas since the spin-1 Ising model can be used for a lattice gas containing molecules that have two orientations: Using X_1 and X_2 as occupation numbers and X_3 holes. Therefore, the first rate constants are $k_{12}=k_{23}=k_1$ which is the insertion or removal of particles associated with translation of particles through the lattices. The second rate constant $k_{13}=k_2$ is associated with reorientation of a molecule at a fixed site. It is assumed that double processes, the simultaneous insertion or removal or rotation of two particles, do not take place, i.e., only single jumps are allowed.

We use recipe II in order to derive the dynamic equations because the general behavior of the solution of the dynamic equations, namely, relaxation curves and also flow diagrams, does not drastically change.[42] Using Eqs. (3), (8), (12), and (14), the set of dynamic equations for the order parameters are obtained:

$$\begin{aligned}
Z_A\frac{dM_A}{k_1dt}&=(k-1)(e_1^A-e_3^A)Q_A\\
&\quad-(ke_1^A+e_2^A+ke_3^A)M_A+(e_1^A-e_3^A),\\
Z_A\frac{dQ_A}{k_1dt}&=-(e_1^A+e_2^A+e_3^A)Q_A+(e_1^A+e_3^A),\\
Z_B\frac{dM_B}{k_1dt}&=(k-1)(e_1^B-e_3^B)Q_B\\
&\quad-(ke_1^B+e_2^B+ke_3^B)M_B+(e_1^B-e_3^B),\\
Z_B\frac{dQ_B}{k_1dt}&=-(e_1^B+e_2^B+e_3^B)Q_B+(e_1^B+e_3^B),
\end{aligned} \tag{15}$$

where $k=k_2/k_1$,

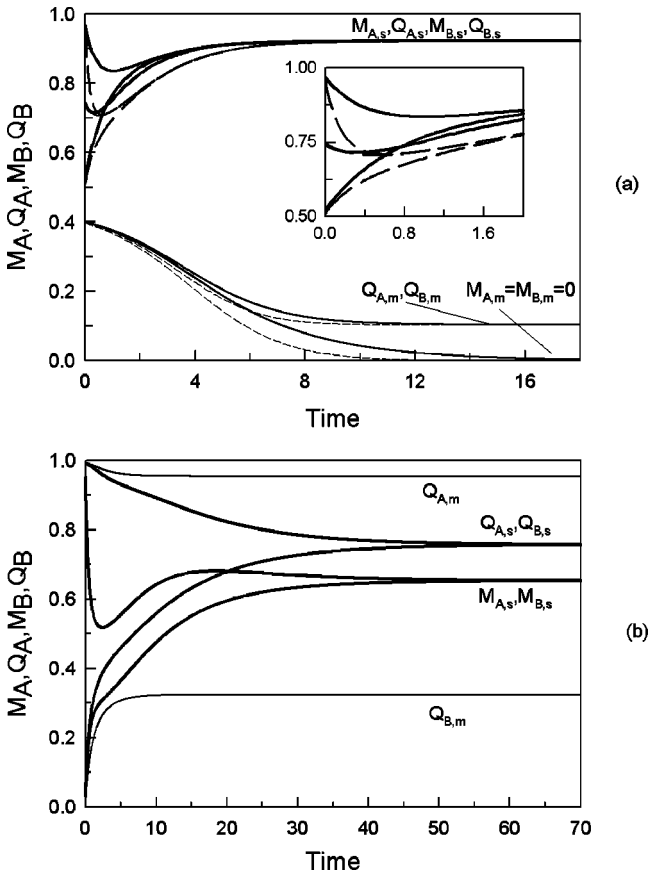

FIG. 7. Relaxation curves of the order parameters M_A, Q_A, M_B, and Q_B for different sets of values of the rate constants: $k_1=k_2=1$ (solid), $k_1=1$ and $k_2=10$ (dashed). Subscript **i** indicates the initial value, **s** the stable state, and **m** the metastable state. (a) For $K/J=-0.15$, $D/J=0.413$, and $kT/J=0.15$. Thick lines are for $M_{A,i}$, $M_{B,i}=0.5$, $M_{B,i}=0.75$, and $Q_{B,i}=0.99$. Thin lines are for $M_{A,i}=Q_{A,i}=M_{B,i}=Q_{B,i}=0.4$. (b) For $K/J=-3.0$, $D/J=-2.15$, and $kT/J=0.5$. Thick lines are for $M_{A,i}=Q_{A,i}=0.99$ and $M_{B,i}=Q_{B,i}=0.01$ and thin lines are for $M_{A,i}=M_{B,i}=0.0$ and $Q_{A,i}=0.99, Q_{B,i}=0.01$.

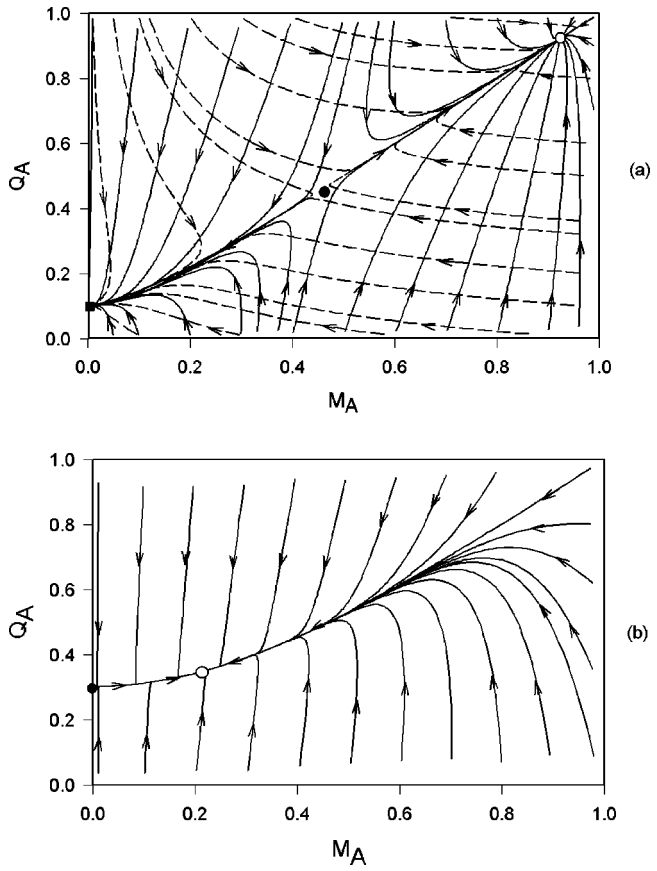

FIG. 8. The flow diagram of the system for two different sets of rate constants (solid) $k_1=k_2=1$ and (dashed) $k_1=1, k_2=10$. The open circle corresponds to the stable state, the filled square to the metastable state, and the filled circle is the unstable state. (a) For $K/J=-0.15$, $D/J=0.413$, and $kT/J=0.15$. (b) For $K/J=-0.15$, $D/J=0.413$, and $kT/J=0.30$.

$$e_i^A=\exp\left(-\frac{\beta}{N}\frac{\partial E}{\partial X_i^A}\right), \quad e_j^B=\exp\left(-\frac{\partial E}{\partial X_i^B}\right),$$

$$Z_A=\sum_{i=1}^{3} e_i^A$$

and

$$Z_B=\sum_{j=1}^{3} e_j^B. \tag{16}$$

These dynamic equations are solved by two different methods: The first one is the Runge-Kutta method. We use this method to study relaxation curves of order parameters and to see the flatness property of the metastable state and as well as the overshooting phenomenon. Relaxation curves of order parameters for several values of D/J, K/J, k_i, and kT/J are plotted in Figs. 7(a) and 7(b). The second one is to express the solution of the equations by means of the flow diagram,[48] which shows the solution of these equations in a two-dimensional phase space of M and Q, starting with initial values very close to boundaries. As time progresses by given small steps, the values of M and Q are computed and the point representing them moves in the plane. A set of the solution curve is obtained by considering all different initial values. The results are presented, for fixed values of D/J, K/J, k_i, and kT/J, in Figs. 8(a) and 8(b). In the figures, the open circle is the stable equilibrium solution which corresponds to the lowest values of the free energy or the deepest minimum, the filled square is the metastable state because the system relaxes into it and it does not correspond to the deepest minimum but corresponds to the secondary minimum, and the filled circle is the unstable solution or state which corresponds to the peak or saddle point. If one studies Fig. 7(a) and Fig. 8(a) ($K/J=-0.15$, $D/J=0.413$, and $kT/J=0.15$) one can see that the system relaxes into only two different states. One is the stable state ($M_{A1}=0.92127$, $M_{B1}=0.92127$; $Q_{A1}=0.92218, Q_{B1}=0.92218$), which corresponds to the lowest value of free energy or the deepest minimum, and the other is the metastable state ($M_{A2}=0.0$, $M_{B2}=0.0$; $Q_{A2}=0.10310, Q_{B2}=0.10310$), which

does not correspond to the deepest minimum but corresponds to the secondary minimum. Moreover, the unstable solution, marked with a filled circle, can be seen explicitly in Fig. 8(a), because it is seen as a saddle point. If one compares Fig. 7(a) and Fig. 8(a) with Fig. 2 for $kT/J=0.15$, one can see that the stable and metastable solutions coincide exactly with each other. Moreover, if one compares only Fig. 8(a) with Fig. 2 for $kT/J=0.15$, one can see that the unstable point, as a separator between the stable and metastable points, coincides with each other one exactly. On the other hand, the system relaxes only one state, i.e., the stable state in Fig. 8(b) ($K/J=-0.15$, $D/J=0.413$, and $kT/J=0.3$), because there do not exist any metastable solutions. If one compares this figure with Fig. 2 for $kT/J=0.3$, one can see that the stable and unstable solutions coincide with each other exactly. If there is some metastable state in the system at this temperature, i.e., $kT/J=0.3$, the system should relax into it, because all the possible initial values are taken. Because we have seen that the system always relaxes into one state, i.e., the stable state, hence there do not exist any metastable states in this case. Furthermore, Fig. 7(b) ($K/J=-3.0$, $D/J=-2.15$, and $kT/J=0.5$) shows the relaxation of the order parameters in which for these K/J and D/J values the stable branches of the order parameters experience three successive second-order phase transitions and the metastable branches of quadrupolar order parameters undergo a single second-order antiquadrupolar phase transition, also see Fig. 5(b). In this case, since the metastable solutions exist besides the stable solutions, the system may also relax into the metastable states. If the initial values are close to the metastable solutions, the system relaxes into it, otherwise into the stable states, seen in Fig. 7(b) explicitly. If one compares Fig. 7(b) with Fig. 5(b) for $kT/J=0.5$, one can see that the stable and metastable solutions coincide with each other exactly. Finally, these facts show us that the solutions and their classifications obtained in the LACVM are complete and correct.

It is worthwhile to mention that following dynamic behaviors have been found from these figures: (i) If the temperature is less than T_u for Figs. 7(a) and 8(a) and less than T_{c2} for Fig. 7(b), the system either relaxes to the stable states or the metastable states and, therefore, relaxation processes depend on the rate constants and the initial values of the order parameters. If the initial values are close to the metastable state, the system always relaxes to the metastable state, otherwise to the stable state, shown in Figs. 7(a) and 8(a). From Figs. 7(a) and 7(b) the ''flatness'' properties of the metastable state[49] are seen clearly, because $Q_{A2}=0.10310$, $Q_{B2}=0.10310$, and $M_{A2}=M_{B2}=0.0$ for Fig. 7(a) and $Q_{A2}=0.95474$, $Q_{B2}=0.32404$, and $M_{A2}=M_{B2}=0.0$ for Fig. 7(b) correspond to the metastable state for which the same results are also found in the equilibrium study, exactly. (ii) If the temperature is greater than $T_{c'}$, the system always relaxes into the disordered states and if the temperature is between T_c and $T_{c'}$ the system always relaxes to the stable state because there do not exist any metastable states in these regions. Therefore, relaxation processes are independent of the rate constants and initial values of the order parameters. It is worthwhile to mention that if the temperature is equal to the critical temperature T_c or $T_{c'}$, the system takes too long a time to relax into the disordered state. This behavior has been also observed in time-dependent one-dimensional spin-1/2 Ising[50] and spin-1 Ising systems.[42,43] Moreover, since $k_2>k_1$ and initial values are not very close to the stable state, the system relaxes into the metastable state more than $k_1=k_2$, seen in Fig. 8(a) explicitly. This fact has been observed experimentally. For example, if one cools some liquid alloys very rapidly, one can obtain amorphous metallic alloys or metallic glasses.[51] Furthermore, one can also see how a system freezes in a metastable state as well as the role of the unstable points as a separator between stable and metastable points. (iii) Since the system has also unstable states, for a number of cases the system tries to go to an unstable state via one of the order parameters, but after some time the relaxation curve makes a sharp turn (a ''U turn,'' so to speak, or an inverse ''U turn,'' seen in Fig. 7) and relaxes to either the stable state or to the metastable state. This is called the ''overshooting'' phenomenon which is often discussed in the glass transition and has also been observed in number of other systems.[31,39,42,43,47]

V. THE METASTABLE PHASE DIAGRAMS IN ADDITION TO THE EQUILIBRIUM PHASE DIAGRAMS

In this section, we present the metastable phase diagrams in addition to the equilibrium phase diagrams of the BEG model for $K/J\leqslant 0$ since we make sure that the metastable branches of the order parameters were obtained completely and correctly in Sec. IV. The critical or second-order phase-transition temperatures for the stable and metastable branches of the order parameters in the case of a second-order phase transition are calculated easily and precisely using the Hessian determinant[14] which is the determination of the second derivative of the free energy with respect to internal or spin variables, namely, X_i and X_j. On the other hand, the first-order phase-transition temperatures for the stable branches of order parameters are found by matching the free-energy values while increasing and decreasing the temperature. The temperature at which the free-energy values equal each other is the first-order phase-transition temperature (T_t) for the stable order parameters. Furthermore, the first-order phase-transition temperature (T_{t2}) for the metastable branches of the order parameters is the temperature where the discontinuity occurs first for M_{A2}, Q_{A2}, M_{B2}, and Q_{B2}.

We can now obtain the metastable and equilibrium phase diagrams of the BEG model and the calculated phase diagrams are presented in Figs. 9(a)–9(f). In these phase diagrams, thick solid and thin dashed lines represent the second- and first-order phase transitions for the stable branches of the order parameters and thin and thick dash-dotted lines indicate the first- and second-order phase transitions of the metastable branches of the order parameters, respectively.

Figure 9(a) shows the phase diagrams in the $(kT/J,D/J)$ plane for $K=0.0$, which is called the Blume-Capel model. As is seen in the figure, besides the ferromagnetic (ordered) phase (f), two different paramagnetic (disordered) phases are found by including the phase transitions of the metastable

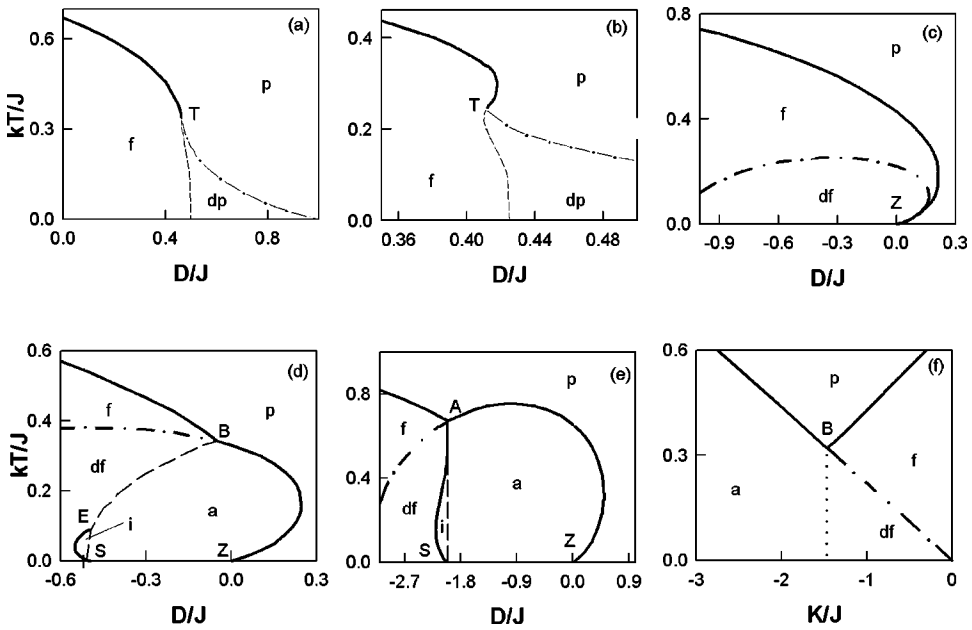

FIG. 9. The equilibrium phase diagrams (thick solid and thin dashed lines) and metastable phase diagrams (thin and thick dash-dotted lines) of the BEG model for K/J and D/J. Thin dashed line and thin dash-dotted line represent the first-order phase transition for the stable and metastable branches of the order parameters, respectively. Thick solid line and thick dash-dotted line represent the second-order phase transition for the stable and metastable branches of the order parameters, respectively. Ferromagnetic (f), dense ferromagnetic (df), ferrimagnetic (i), antiquadrupolar (a), paramagnetic (p), and dense paramagnetic (dp) phases are found. The special points are tricritical (T), bicritical (B), multicritical (A), critical end point (E), zero-temperature highly degenerate (S), and zero-temperature critical (Z). (a) $K/J=0.0$. (b) $K/J=-0.15$. (c) $K/J=-1.0$. (d) $K/J=-1.5$. (e) $K/J=-3.0$. (f) $D/J=0.0$.

branches of the order parameters, namely, M_{A2}, M_{B2}, Q_{A2}, and Q_{B2}. (i) The pure paramagnetic (p) phase as seen with only the stable branch of the quadrupolar order parameters, Q_{A1} and Q_{B1}. (ii) The dense paramagnetic (dp) phase with the metastable and unstable branches of order parameters occur besides Q_{A1} and Q_{B1}. The p and dp can also be defined as follows: p is a region where the only solution is the paramagnetic solution, i.e., $M_A=M_B=0$, while in the dp region this paramagnetic phase can coexist on sufficiently short-time scales with another less symmetrical locally stable phase, i.e., the metastable phase. Moreover, in the dp region the unstable solutions of the order parameters also exist. The boundary of the pure and dense paramagnetic phases (thin dash-dotted line) is the first-order line for the metastable branches of the order parameters that starts at $D/J=1.0$ and ends at T in which is the tricritical point where the second-order phase-transition line turns to a first-order one.

We turn to the very interesting case when the biquadratic (K) and bilinear exchange interactions (J) have opposite signs. Figure 9(b) illustrates the metastable phase diagram in addition to the equilibrium phase diagram for $K/J=-0.15$. This phase diagram is similar to the phase diagram given in Fig. 9(a), except a double reentrant behavior takes place in the system. For the range of $0.411 \leqslant D/J \leqslant 0.418$, the system exhibits the f-p-f-p successive phase transitions as the temperature is increased. As value of K/J increases in the negative value, and eventually the tricritical point disappears as seen in Fig. 9(c). In Fig. 9(c) three main regions appear in the system. (p) represents a disordered state or paramagnetic phase of the system with $M_{A1}=M_{B1}=0$ and $Q_{A1}=Q_{B1} \neq 0$. (f) denotes pure ferromagnetic phase in which the stable branches of the order parameters exist (sometimes unstable branches also occur, e.g., as seen in Fig. 6). (df) represents a dense ferromagnetic phase and in this region the metastable and unstable branches of the order parameters also exist besides the stable quadrupolar order parameters, Q_{A1} and Q_{B1}. Moreover, the second-order phase line for the metastable branches of the order parameters (thick dash-dotted line) separates the (f) phase from the (df) phase. In this phase diagram, the special point is only the zero-temperature critical (Z) point and the equilibrium phase diagram shows a reentrant behavior in which the reentrant behavior starts for the first time at Z and appears in the range of the $0<D/J<0.22$. On the other hand, the metastable phase diagram also illustrates the reentrant behavior in the range of the $0<D/J<0.166$. Figure 9(d) represents the metastable phase diagram in addition to the equilibrium phase diagram for $K/J=-1.5$. In the phase diagram, the antiquadrupolar (a) phase is separated from the paramagnetic (p) phase by two second-order phase lines that meet at a bicritical point (B). The antiquadrupolar (a) phase is also separated from the dense ferromagnetic (df) and ferrimagnetic (i) phases by the first-order phase-transition line. Moreover, (df) and (i) phases are separated by the other second-order phase line starting at the zero-temperature highly degenerate point (S) and terminating at the critical end point (E). For more negative values of biquadratic interaction such as $K/J=-3.0$ the phase diagram of the system becomes more interesting. The phase diagram for $K/J=-3.0$ is illustrated in Fig. 9(e). The

phase diagram is similar to the phase diagram of Fig. 9(d), except the critical end point (E) in Fig. 9(d) disappears or it joins to a multicritical point (A), seen in Fig. 9(e). Finally, Fig. 9(f) illustrates the phase diagram of the BEG model in the ($kT/J,K/J$) plane for $D/J=0.0$. In the phase diagram, the four different regions have been seen, namely, (p), (a), (df), and (f). The second-order phase-transition lines for the stable branch of the order parameters (thick solid lines) separate (a), (p), and (f) phases. Moreover, the second-order phase line for the metastable branches of the order parameters (thick dash-dotted line) separates (f) and (df) phases. On the other hand, the dotted line separates the (a) phase from the (df) phase. It should be mentioned that (f) and (df) can also be defined as follows: (f) is a region where the only solution is the ferromagnetic solution (sometimes unstable solutions also occur), i.e., $M_A, M_B=0, Q_A, Q_B\neq 0$, while in the df region this ferromagnetic phase can coexist on sufficiently short-time scales with another less symmetrical locally stable phase.

In conclusion, all the equilibrium phase diagrams of the system are exactly the same as the equilibrium phase diagrams of Hoston and Berker.[15] However, we have also obtained and presented the metastable phase diagrams of the BEG model in addition to the equilibrium phase diagrams.

VI. SUMMARY AND CONCLUSION

In this work, we have investigated the thermal variations of the order parameters of the spin-1 Ising BEG model with the repulsive biquadratic interaction by using the LACVM. Besides the stable branches of the order parameters, we obtained the metastable and unstable parts of these curves, and phase transitions of the metastable branches of the order parameters were also found. The classification of the stable, metastable, and unstable states is made by matching the free-energy values of these solutions. We also studied the dynamics of the model by the path probability method in order to make sure that we have found and defined the metastable and unstable branches of the order parameters completely and correctly. Then, we presented the multicritical phase diagrams of the BEG model including the phase transitions of metastable branches of the order parameters. Therefore, we presented the metastable phase diagram in addition to the equilibrium phase diagram for the BEG model with the repulsive biquadratic interaction. We found that the equilibrium phase diagrams of the system are exactly the same as the equilibrium phase diagrams of Hoston and Berker.[15] However, the main difference is about the paramagnetic and ferromagnetic phases as follows: We found two different paramagnetic and ferromagnetic phases which we called a pure paramagnetic (p) phase with $M_{A1}=M_{B1}=0, Q_{A1}=Q_{B1}$ and a pure ferromagnetic (f) phase with the stable branches of the order parameters, i.e., $M_{A1}=M_{B1}\neq 0, Q_{A1}=Q_{B1}$, and a dense paramagnetic phase (dp) with the metastable and unstable branches of order parameters existing besides $Q_{A1}=Q_{B1}$ and dense ferromagnetic phase (df) with the stable, metastable, and unstable branches of the order parameters. In the phase diagrams, the first-order phase lines (thin dash-dotted lines) for the metastable branches of the order parameters separate the (p) phase from the (dp) phase, seen in Figs. 9(a) and 9(b). On the other hand, the second-order phase lines (thick dash-dotted lines) for the metastable branches of the order parameters separate the (f) phase from the (df) phase, seen in Figs. 9(c)–9(f).

Finally, it is worthwhile to mention that we have found that the metastable phase diagrams of the BEG model for $K/J\leqslant 0$, which has served as a paradigm for a large number of physically important phenomena, always exists at the low temperatures that are consistent with experimental and theoretical works on some alloys,[24–26] semiconductors,[27,28] polymers,[29] water,[30] and the ternary system.[31]

ACKNOWLEDGMENTS

This work was supported by the Research Fund of Erciyes University, Grant No. 00-052-6.

[1] M. Blume, V. J. Emery, and R. B. Griffiths, Phys. Rev. A **4**, 1071 (1971).
[2] J. Lajzerowicz and J. Sivardière, Phys. Rev. A **11**, 2079 (1975); J. Sivardiére and J. Lajzerowicz, *ibid.* **11**, 2090 (1975); **11**, 2101 (1975).
[3] D. Mukamel and M. Blume, Phys. Rev. A **10**, 610 (1974).
[4] A. N. Berker and M. Wortis, Phys. Rev. B **14**, 4946 (1976).
[5] J. W. Tucker, J. Magn. Magn. Mater. **71**, 27 (1987).
[6] C. Buzano and A. Pelizzola, Physica A **195**, 197 (1993).
[7] D. M. Saul, M. Wortis, and D. Stauffer, Phys. Rev. B **9**, 4964 (1974).
[8] Z. Koza, C. Jasuukiewicz, and A. Pekalski, Physica A **164**, 191 (1990).
[9] K. Takahashi and M. Tanaka, J. Phys. Soc. Jpn. **46**, 1428 (1979); **48**, 1423 (1980).
[10] E. Albayrak and M. Keskin, J. Magn. Magn. Mater. **203**, 201 (2000).
[11] K. G. Chakraborty and J. W. Tucker, J. Magn. Magn. Mater. **54**, 1349 (1986).
[12] M. Keskin, C. Ekiz, and O. Yalçin Physica A **267**, 392 (1999).
[13] M. Keskin and C. Ekiz, J. Chem. Phys. **113**, 5407 (2000).
[14] H. H. Chen and P. M. Levy, Phys. Rev. B **7**, 4267 (1973).
[15] W. Hoston and A. N. Berker, Phys. Rev. Lett. **67**, 1027 (1991).
[16] W. Hoston and A. N. Berker, J. Appl. Phys. **70**, 6101 (1991).
[17] M. Tanaka and T. Kawabe, J. Phys. Soc. Jpn. **54**, 2194 (1985); Y. L. Wang and C. Wenthworth, J. Appl. Phys. **61**, 4411 (1987); Y. L. Wang, F. Lee, and J. D. Kimel, Phys. Rev. B **36**, 8945 (1987).
[18] G. Grigelionis and A. Rosengren, Physica A **208**, 287 (1994); S. Lapinskas and A. Rosengren, Phys. Rev. B **49**, 15190 (1994); J. W. Tucker, T. Balcerzak, M. Gzik, and A. Sukiennicki, J. Magn. Magn. Mater. **187**, 381 (1998).
[19] R. R. Netz, Europhys. Lett. **17**, 373 (1992).
[20] A. Z. Akheyan and N. S. Ananikian, J. Phys. A **29**, 721 (1996).
[21] M. Keskin and Ş. Özgan, Phys. Lett. A **145**, 340 (1990); M.

Keskin, M. Arı, and Ş. Özgan, Tr. J. Phys. **15**, 575 (1991); M. Keskin, and A. Erdinç, Tr. J. Phys. **19**, 88 (1995); C. Temirci, A. Kökçe, and M. Keskin, Physica A **231**, 673 (1996).
[22] M. Keskin, Phys. Scr. **47**, 328 (1993).
[23] M. Keskin and H. Arslan, J. Magn. Magn. Mater. **146**, L247 (1995); M. Keskin and H. Arslan, Tr. J. Phys. **19**, 408 (1995).
[24] S. Nourbakhsh and P. Chen, Acta Metall. **37**, 1573 (1989); H. J. Fecht, Acta Metall. Mater. **39**, 1003 (1991); C. Michaelsen, Z. H. Yan, and R. Bormann, J. Appl. Phys. **73**, 2249 (1993); W. Loser, R. Hermann, M. Leonhardt, D. Stephan, and R. Bormann, Mater. Sci. Eng., A **224**, 53 (1997).
[25] J. M. Sanchez, M. C. Cadeville, V. Pierron-Bohnes, and G. Inden, Phys. Rev. B **54**, 8958 (1996).
[26] E. Obradó, C. Frontera, L. Mañosa, and A. Planes, Phys. Rev. B **58**, 14245 (1998).
[27] J. Ni and B. L. Gu, Solid State Commun. **83**, 757 (1992).
[28] K. E. Newman and J. D. Dow, Phys. Rev. B **27**, 7495 (1983).
[29] V. Mishra and H. Sperling, Polym. Bull. (Berlin) **36**, 3593 (1995).
[30] E. G. Ponyatovsky, V. V. Sinitsyn, and T. A. Pozdnyakova, J. Chem. Phys. **109**, 2413 (1998); P. G. Debenedetti, *Metastable Liquids* (Princeton University Press, Princeton, NJ, 1996).
[31] J. Ni and B. L. Gu, Phys. Rev. Lett. **79**, 3922 (1997).
[32] R. Osório, S. Froyen, and A. Zunger, Solid State Commun. **78**, 249 (1991).
[33] R. Kikuchi, Phys. Rev. **81**, 988 (1951).
[34] See, e.g., W. H. Press, B. P. Flannery, S. A. Teukolsky, and W. T. Vetterling, *Numerical Recipes* (Cambridge University, London, 1986); G. E. Forsythe, M. A. Malcolm, and C. B. Moler, *Computer Methods for Mathematical Computations* (Prentice-Hall, Englewood Cliffs, NJ, 1977).
[35] R. Kikuchi, Suppl. Prog. Theor. Phys. **35**, 1 (1966).
[36] K. Wada, M. Kaburagi, T. Uchida, and R. Kikuchi, J. Stat. Phys. **53**, 1081 (1988).
[37] R. Kikuchi and H. Sato, J. Chem. Phys. **51**, 161 (1969); **53**, 2702 (1970).
[38] H. Sato and R. Kikuchi, J. Chem. Phys. **55**, 677 (1971).
[39] H. Sato and R. Kikuchi, Acta Metall. **24**, 797 (1976); K. Gschwend, H. Sato, and R. Kikuchi, J. Chem. Phys. **69**, 5006 (1978).
[40] Z. Qin, A. R. Allnatt, and E. L. Allnatt, J. Phys.: Condens. Matter **10**, 5295 (1998).
[41] P. H. E. Meijer, M. Keskin, and E. Bodegom, J. Stat. Phys. **45**, 215 (1986).
[42] M. Keskin and P. H. E. Meijer, Physica A **122**, 1 (1983).
[43] M. Keskin, Physica A **135**, 226 (1986); M. Keskin and P. H. E. Meijer, J. Chem. Phys. **85**, 7324 (1986); M. Keskin, M. Arı, and P. H. E. Meijer, Physica A **157**, 1000 (1989); M. Keskin and R. Erdem, J. Stat. Phys. **89**, 1035 (1997); M. Keskin and A. Solak, J. Chem. Phys. **112**, 6396 (2000); A. Erdinç and M. Keskin, Physica A **307**, 453 (2002).
[44] T. Mohri and S. Miyagishima, Mater. Trans., JIM **39**, 154 (1998).
[45] J. Ni and B. L. Gu, Phys. Rev. Lett. **79**, 3922 (1997).
[46] H. Ohmi, T. Uchida, and K. Wada, Jpn. J. Appl. Phys., Part 1 **35**, 226 (1996).
[47] C. C. Wang, K. S. Goto, and S. A. Akbar, J. Electrochem. Soc. **139**, 2807 (1993).
[48] J. Cunningham, Am. Sci. **51**, 427 (1963); M. Minorski, *Nonlinear Oscillations* (Van Nostrand Reinhold, New York, 1962).
[49] K. Binder, Phys. Rev. B **8**, 3423 (1973).
[50] H. E. Stanley, *Introduction to Phase Transitions and Critical Phenomena* (Oxford University Press, New York, 1971).
[51] H. Jones, Rapid Solidification of Metals and Alloys, (Institute of Metallurgists, London, 1982); *Amorphous Metallic Alloys*, edited by F. E. Luborsky (Butterworths, London, 1983); *Rapid Solidification Technology*, edited by R. L. Ashbrook (American Society for Metals, Metals Park, OH, 1983).